Use of GOES IR Data in Estimating Synoptic-Scale Rainfall: Algorithm Development and Transferability

Franklin R. Robertson

Atmospheric Sciences Division

NASA Marshall Space Flight Center

Huntsville, AL 35812

To be submitted to

Journal of Climate and Applied Meteorology

March 1986

ABSTRACT

Hourly reporting raingauge data and GOES infrared (IR) geostationary satellite imagery are used to develop a technique for rain estimates that does not depend on any a priori brightness temperature threshold specifications. A second-order polynomial is fitted to the 1164 hourly raingauge/IR image pairs. The resulting algorithm is investigated using independent data to determine: 1) the effect of spatial and temporal averaging to reduce random error and, 2) the problems associated with transferring the algorithm from its development location (coastal U.S.) to open-ocean regions.

Applications to the GATE B-Scale array during a portion of Phase III suggests a level of skill comparable to that of an optimal thresholding method developed explicitly for GATE. For 12h, area averaged rain estimates over North Carolina during passage of winter extratropical cyclones, a drop in correlation with ground truth is noted in comparison to tropical climates (.71 versus .85, respectively). Comparison of point satellite estimates in the South Pacific suggests an over-estimate of about 20 percent. The results are interpreted as encouraging for transfer of indirect (IR or visible) algorithms between regions of similar climate.

I. Introduction

Estimating rainfall using infrared (IR) and/or visible satellite imagery has met with varying degrees of success depending on the spatial and temporal resolution attempted and the synoptic regime considered. Kilonsky and Ramage (1976), Lovejoy and Austin (1979a), Arkin (1979), and Richards and Arkin (1981), have demonstrated that, for time and space scales that are large compared to those of individual convective elements, tropical deep convective rainfall is well correlated with high cold clouds. Treatment of middle-latitude rain systems associated with baroclinic waves has been less successful. Wylie (1979), in examining rain estimation from visible and IR measurements over Montreal, found it necessary to incorporate a one-dimensional cloud model to obtain accuracies of about a factor of 2. His results represent averages over approximately three-hour periods and areas on the order of 10^5 square kilometers. Lovejoy and Austin (1979b), applied a pattern recognition scheme whereby an optimum boundary was found to separate raining and non-raining points in the visible/IR plane. This method was effective in convective situations but showed less skill in the single stratiform case considered.

All the above methods can be classified as "indirect" since IR and visible imaging sensors respond primarily to suspended hydrometeors and not to precipitation-size particles. The physical basis for the skill of such methods lies mainly in the

fact that cold high clouds are often produced by precipitating convective cells and are signatures of upward motion in a locally saturated atmosphere. Life history schemes (e.g. Griffith, et al., 1978), and Stout et al., 1979), consider temporal changes in cloud top structure to infer distribution of precipitation on the scale of individual convective clouds. The necessity of this detail in attempting rain estimates of 6 hours or more has recently been called into question (Richards and Arkin, 1981, Negri et al., 1984). Lovejoy and Austin (1979a), have argued convincingly that the strength of all indirect schemes lies in discriminating raining versus non-raining clouds; substantially less skill exists in actual rain rate determination.

Despite a lack of explicit physics in the indirect approach, there is continued strong interest for a number of reasons: 1) archives of geostationary and polar orbiter visible/IR imagery are extensive and availability of these data for research and operational interests seems assured for the foreseeable future, 2) indirect methods are relatively simple to program and can provide precipitation estimates whose errors are consistent with the accuracy of upper-air data used in many diagnostic calculations, 3) although passive microwave methods (Wilheit et al., 1977; Spencer, 1984), offer a more physical basis for rain estimates, infrequent data coverage from low earth orbits and uncertainties as to availability beyond the Nimbus 7 SMMR (Scanning Multichannel Microwave Radiometer) present some problems.

With growing interest in all aspects of the global hydrological cycle and the dynamics of planetary-scale events such as the El Nino/Southern Oscillation, there is a need to extend the applicability of indirect methods to a variety of climates--oceanic environments in particular. The purpose of this study is to develop a rainfall estimation technique with geostationary IR imagery and raingauge data and to investigate the transferability of the algorithm from its developmental region (coastal Southeast U.S.) to an open-ocean environment. Both tropical and middle-latitude rain systems are to be incorporated into the developmental data set. Although the performance of indirect schemes is generally suspect in the stratiform precipitation characteristic of middle-latitude cyclones, it appears that little quantitative evaluation of algorithms in this environment has been done. Since convective elements embedded within stratiform rain might contribute significantly to total rainfall in these situations, indirect methods should exhibit some level of skill. Specifically, this paper addresses precipitation estimates on time and space on the order of 12 hours and 10^5 square kilometers, i.e., synoptic-scale resolution. Estimates of this scale should be compatible with diagnostic heat and moisture budgets derived from FGGE (First Global Atmospheric Research Program Global Experiment) data analyses. In section 2, a description of the methodology and data is presented along with a discussion of the resulting algorithm. Section 3 contains an evaluation of the performance

of the algorithm when applied to locations other than where it was developed. Included in this test are instances of deep tropical convection over the GATE (Global Atmospheric Research Program Atlantic Tropical Experiment) B-Scale Array, the tropical South Pacific Ocean and middle-latitude stratiform rain with embedded convection over coastal North Carolina during winter. A summary of the results and discussion of the potential usefulness of this approach are given in section 4.

2. Algorithm Development

a. Methodology and Data

Most indirect techniques rely upon an equivalent black body temperature threshold temperature to separate raining from non-raining clouds. In the simplest formulation, the area mean rainrate over a computational region is then assumed proportional to the fractional coverage by clouds colder or brighter than this threshold. For deep tropical convection, IR thresholds between about 253 K (Griffith et al., 1978), and 235 K (Arkin, 1979), have been most commonly used. In considering IR threshold versus rainfall algorithm performance, Stout et al., (1979), and Richards and Arkin (1981), have found that during GATE the best correlation lies in the range 235 to 240 K. If an IR method is to be extended to cover instances where embedded convection and stratiform rain are present, some means of recognizing warmer rain-producing clouds is necessary. The procedure adopted in this study is to seek a statistical relationship between gauge-

observed precipitation at the ground and the equivalent black body temperature, T_b, of the GOES IR pixels corresponding to the gauge locations. For convenience, this approach will be referred to as pixel indexing (PI) since it associates a point rainrate measurement with the T_b value for a given pixel. An algorithm developed from this data set is then used to construct rainrate estimates through appropriate temporal and spatial averaging. Since the PI technique results in a function which assigns a rainrate to each T_b value, it allows for the possibility of raining clouds whose tops are warmer than most commonly used thresholds. One would naturally expect correlation at this pixel-scale to be low due to a number of random error sources. The validity of the working premise that the errors are indeed random and can be minimized by appropriate space and time averaging will be examined in section 3.

Although calibrated C-band radars provided ground truth data for tropical oceanic rainfall gathered during GATE (Hudlow and Patterson, 1979), satisfactory observations of rainfall rates over oceans for other climate regimes, including that of middle-latitude wave cyclones, are not readily available. For this reason, hourly rainfall measurements at coastal raingauge locations were used to provide ground truth (Fig. 1). Observed rainfall amounts were extracted from the hourly precipitation data (HPD) summaries produced by the National Climatic Center, Asheville, North Carolina. Synoptic situations selected for the data base included Gulf Coast easterly waves, closed upper-level

lows, warm and cold frontal passages and convection associated with diurnal heating. Although the influence of a non-oceanic location cannot be discounted a priori, it will be shown that transferring the algorithm to several other locations produces smaller biases than one might suppose. Digital IR imagery for developing the algorithm consisted of hourly GOES East and West 8 km resolution data obtained from the Environemntal Data Information Service at the University of Wisconsin. All GOES data handling was performed on the Harris/6 McIDAS (Man computer Interactive Data Acquisition System) resident at the Marshall Space Flight Center. A total of 1164 pairs of hourly rain amount and IR temperature was obtained.

b. Resulting algorithm

A scatter diagram of hourly rain amount versus IR T_b is shown in Fig. 2. The most prominent aspects of this relationship are the substantial scatter and the existence of zero rainrates for the entire range of temperatures. Along the top of Fig. 2, the percentage of observations reporting rainfall is plotted for 5 K intervals. A sharp increase in the percentage of raining points corresponding to the interval 245 to 235 K verifies the prominent binary (rain/no rain) signal that forms the basis for thresholding methods. A least squares analysis was performed to fit the data with a quadratic polynomial:

$$\text{Rain rate (mm/hr)} = 7.04 - 11.10T^* + 4.26T^{*2}, \qquad (1)$$

where

$$T^* = (T_b - 200)/50 \qquad (2)$$

Correlations of satellite temperature versus observed hourly rainrate is -.36. The resulting curve in Fig. 2 intersects the abcissa near T_b=255K; thus rainrates are effectively zero above this temperature. The slope of the curve becomes small for temperature warmer than about 235 K. The choice of a quadratic fit is somewhat arbitrary. A linear fit gave a correlation of -.31. Expressions higher than order 2 could be constructed for this developmental data set but the stability of these expressions when applied to independent data sets would likely be diminished. As noted in section 1, an inherent physical weakness of the IR approach is the fact that the sensor responds primarily to suspended hydrometeors; therefore, there is only an indirect relationship between what is actually sensed and the variable one wishes to predict. Warm low clouds generally are not deep enough to produce sufficient condensate for heavy rainrates. In Fig. 2, only one instance of rain >20 mm/hr is found for T_b>240 K. On the other hand, high clouds may be associated with cores of heavy precipitating convection, steady anvil rain, non-raining convective debris or cirrus from baroclinic waves. Both the observed rain amounts and the percentage of points reporting rain increase with decreasing T_b. Still, approximately one-third of

the points colder than 225 K report no rain. Clearly, one can expect to use the derived relationship only if there exists a substantial component of random error that can be reduced through space and/or time averaging. Among the most likely contributors to random error are gauge sampling, satellite navigation and rain cell life-cycle effects. The precipitation processes averaged over the IR pixel area (64 km^2) are assumed to be adequately sampled by a single raingauge measurement. This assumption is often likely to be a poor one since it is well known that there is substantial horizontal structure in convective rainrates on the scale of an individual rain cell which is similar itself in size to the IR pixel. An analogous problem with temporal sampling occurs since each hour-long raingauge accumulation is paired with an instantaneous IR measurement. Related to this problem is an additional uncertainty arising from satellite navigation errors. Typical errors in location are in the range of 10 to 15 km and, in some cases, may be twice as large.

The most serious uncertainties are likely to arise because of life-cycle effects. For individual convective towers, cloud areal extent generally lags behind rainfall rate (Griffith, et al., 1978). This effect is quite prominent in mesoscale convective systems. Furthermore, horizontal structure in rainfall rates may vary substantially throughout an individual cloud, but bear little resemblance to structure in cloud-top temperatures. In particular, the upshear portions of deep convective clouds are likely to produce heavier rainrates than

downshear regions (Scofield and Oliver, 1977). There is considerable evidence that life cycle effects can be minimized if spatial and temporal resolution are sacrificed. Richards and Arkin (1981), noted that for averaging scales of 2 to 3 degrees latitude x longitude and periods 6 hours or longer, a simple linear thresholding approach yielded accuracies comparable to the life history methods of Griffith, et al., and Stout, et al., (1979). In evaluating the contribution of various terms in the Griffith, et al., method, Negri, et al., (1984) conclude that the approach is unnecessarily complicated for estimating daily rainfall. They found that a modified non-life history version yielded comparable error characteristics. Since averaging over areas $>10^5$ square kilometers and 6-12 hours would encompass many convective cells and their cloud debris at various phases in their life cycles, it is also reasonable to expect a reduction in the random component of error in the PI algorithm.

3. Tests on Independent Data

To apply the algorithm with reasonable confidence to a variety of oceanic climates, two issues must be addressed: 1) quantifying the effect of synoptic time and space averaging in reducing random error and 2) the nature of any bias that may be introduced in transferring the algorithm from coastal to open-ocean locations. We explore these questions in this section by testing the algorithm on three independent data sets.

a. GATE Phase III

The most accurate precipitation measurements available over tropical oceans are those collected during GATE. Seven days of Phase III SMS-1/GOES digital IR imagery were obtained through the courtesy of Dr. David Martin, University of Wisconsin. Rainrate estimates were performed on an hourly basis by evaluating (1) at each 4 km pixel and then area-averaging over the B-Scale Array. Verification consisted of the hourly radar rainfall amounts from the C-Band radar network compiled by Hudlow and Patterson (1979). A time plot of estimated and radar-observed rainfall is given in Fig. 3. The satellite estimate performs quite well for most events although significant overestimates (4 September and underestimates (9 September) are noted. The results are summarized statistically in Table 1 for a temporal averaging scale of 12 hours. Many of the events studied occurred on days when less than 24 hours of satellite imagery were available. Averaging was performed starting with the first available data of a given day and remaining data with less than 6h coverage was not considered. Root mean square errors in Table 1 suggest that for about 95 percent of the 12h averages (two standard deviations) the errors should be less than a factor of 2. Since a bias of 1.0 is a perfect score, a slight systematic overestimation of rainfall is indicated. A correlation of .85 for the 12h averaging demonstrates the substantial effect of spatial and temporal smoothing. Recall that in section 2, point

estimates of hourly rainfall used in developing the algorithm correlated with individual gauge measurements at only .36.

To investigate more fully the question of transferability, the PI method is compared with one developed specifically for GATE. Arkin (1979) sought the optimum one-parameter linear model that could be derived for each of the three phases of GATE. Using a threshold of 235 K, he related fractional high cloud coverage in a 2.5 degree square to the radar rainrates of Hudlow and Patterson (1979). Applying Arkin's technique to the B-Scale hexagon, one obtains the estimates shown in Fig. 4. The results are quite similar to those of the PI method--both do well on 2 and 5 September, but experience difficulty on 4 and 9 September. The correlation coefficient for Arkin's method in Table 2 suggests only a slightly higher level of skill with .89 as compared to .85 from the PI method. Although the root mean square error is lower, the bias is somewhat higher. The significance of this comparison is the fact that the present algorithm, which was developed with data along the coastal U.S., performs nearly as well as a method developed explicitly for Phase III of GATE. This finding is not unexpected since Woodley, et al., 1980), successfully applied their method developed with observations over Florida to the GATE region. If this type result could be shown representative, problems associated with the transferability of the algorithm to tropical open-ocean regimes would not appear to be major.

b. Coastal North Carolina

In this section the algorithm is tested in several instances of precipitation accompanying middle-latitude wave cyclones. Unfortunately, there exists little reliable documentation of open-ocean rainfall determined from calibrated radars. Consequently, a network of hourly and daily raingauges over coastal North Carolina was chosen as the test region (Fig. 5). Lack of a true oceanic climate limits the conclusions that can be drawn regarding transferability, but enables an adequate sampling of extratropical waves. Since stratiform rain is not surface-rooted as is most deep convection, one might expect rain estimates in baroclinic waves to be less sensitive to oceanic versus continental exposure than predominantly convective systems. Areal mean rainrates were determined for 12 and 24 hour periods during eight days in January and February. In constructing 12h verification, the 24h total rain of each daily reporting gauge was assumed to fall with the same temporal distribution as that of the nearest hourly reporting gauge. Since gauge density over the area in Fig. 5 was fairly uniform, area-average rainrates were determined as simple averages of the reported gauge amounts. Hourly, full resolution GOES IR imagery was again used to produce 12h and 24h rain rate estimates for each pixel; the results were then averaged over the entire network. Figure 6 shows satellite estimates and corresponding gauge rainrates for eight 24h periods. A statistical summary is presented in Table 2. Compared to the GATE results, there is a

notable decline in skill with 12 and 24h correlations dropping to .71 and .78, respectively. For many of the 24h periods in Fig. 6, significant overestimates in rainrate occur in the first 12 hours (21 January, 7 February 1979, 6 February 1983). Similarly, a tendency to underestimate rainfall is noted for 12h periods which correspond to passage of the western portion of the synoptic-scale cloud shield (21 January, 19 February 1979, 6 February 1983). This systematically incorrect diagnosis of rain is caused by widespread regions of cold cirrus preceding the cyclones and is manifest in the 12h bias score which is substantially larger than for 24h averaging.

Rain estimates using the Arkin (1979) technique were also produced for comparison (Fig. 7). Overall skill in the two methods is comparable. The PI method has slightly higher correlation rates for 24h averaging while the Arkin method is slightly better at 12h. Arkin's method produces a larger bias and a larger root mean square error. Of course, it is not strictly appropriate to apply a method developed specifically for GATE Phase III to a middle-latitude environment. For operational use in producing monthly global rainfall estimates, Arkin (1983), has used the pooled data for all three phases of GATE and set the y-intercept of the linear equation relating rainfall and fractional cloud cover to zero. The resulting algorithm, termed the GOES Precipitation Index (GPI), gives a precipitation rate of 2.96 mm/h for clouds colder than 235 K--slightly smaller than the Phase III algorithm of 3.08 mm/hr. Applying the GPI to the North

Carolina data set reduces the root mean square errors to .53 and .37 for 12 and 24h averages, respectively.

c. South Pacific Islands

In a study currently underway, the initial application of the PI method will be an assessment of rainfall in the South Pacific Convergence Zone (SPCZ). Ultimately, 12h rain estimates will be produced over a domain bounded by 10 N, 50 S, 120 W, and 170 E at a resolution of 2.5 degrees. To reduce data handling to a manageable size, three-hourly GOES W IR imagery at 16 km resolution is being used. Preliminary tests have indicated that a reduction from full resolution of 4X8 km and one-half hour frequency produces little change in estimated 12 and 24h rain rates for 2.5 degree squares. In this section, we utilize the existing surface synoptic rainfall observations in the South Pacific in a further assessment of transferability. Although this region is notably data poor, a number of island stations reporting precipitation were available during FGGE. While station density precludes a determination of meaningful areal rainrates, the gauge and satellite amounts can be compared to detect overall biases. Nine consecutive days of rainfall data were used in this test. For each 12h period beginning at 0000 and 1200 GMT, observed rainrates were extracted from synoptic reports at the gauge locations shown in Fig. 7. IR imagery at 3h intervals was also used to produce 12h mean rainrates at each gauge location. Rainrates for each 12h period were then averaged

over all 43 station locations. During the nine-day period, the northwest portion of the network is influenced by tropical deep convection. The stations to the southeast experienced deep convection and stratiform rain associated with transient wave cyclones (Vincent, 1985). Comparison of gauge to satellite estimates in Fig. 8 shows the time series of gauge-observed rainfall and the satellite estimates produced by the PI and Arkin algorithms. A statistical summary is given in Table 3. Both satellite estimates provide generally fair indications of temporal variations with the PI estimate providing a somewhat higher correlation of .74 versus .68 for the Arkin method. The former is more indicative of the heavier rainfall events in the 12h periods beginning at 1200 GMT, 13 and 14 January, but also overpredicts at 1200 GMT, 16 January. One would expect that with further area averaging associated in producing 2.5° latitude x longitude estimates, the correlation rate might approach the GATE result. This hypothesis could not, of course, be tested with the current paucity of surface data in the SPCZ. RMS error is comparable for the two methods but the bias is higher for the PI, reflecting the overestimate of .19 mm/h compared to an underestimate of .08 mm/h for Arkin's method. The bias in the PI may be linked to a preponderance of very cold T_b's which frequently were as cold as 190 K. None of the developmental data points were this cold (nor those during GATE). These cold cloud top events are, therefore, not well represented and are a severe test for both algorithms. Presumably, the GATE Phase III

algorithm is not as sensitive as the PI method to extremes of cloud height since it is a thresholding scheme. It is reasonable to expect that the errors reported here are probably representative of most extreme events because of the unusually cold cloud top temperatures. Both schemes can be adjusted by an appropriate scaling factor to eliminate the difference between the estimated and observed amounts. These results are also given in Table 3. The higher correlation of the PI method allows an adjustment which produces the lowest bias and RMS error. Obviously, this comparison must be interpreted with care because of the small sample size.

4. Discussion and Conclusions

An algorithm to estimate synoptic-scale rainfall has been developed using GOES IR imagery and individual hourly raingauge reports. In a general sense, the results of the test on independent data demonstrate the feasibility of using point rainfall measurements in developing a method to be applied to synoptic space and time scales. As expected, correlation between IR T_b and observed rainfall was low (-.36) in the developmental data set primarily due to random error. Through synoptic space and time, averaging correlations in the range of .71 to .85 were produced by the PI algorithm in tests on independent cases.

For the three tests performed in this study, transferring the algorithm from its location of development to other climates

produced modest impact. Differences in mean observed and estimated rainfall rates in Tables 1 and 2 were in the neighborhood of 10 to 15 percent or less. In the test involving the Pacific Island data, an overestimate of about 20 percent was found. In tests over coastal North Carolina, a systematic error was found due apparently to cirrus shields ahead of the wave cyclones. The suggestion of underestimating was noted on the western side of cloud shields. The reason for this is not clear but it is interesting to note that in the GATE and North Carolina tests, the PI and Arkin methods performed with essentially equal skill. One might speculate that this is because both methods are "indexing" schemes in that they relate rainrate to IR T_b for a single image and do not recognize mesoscale sloping updrafts frequently present in baroclinic extratropical cyclones (Emanuel, 1983). Future improvements to the PI algorithm might be obtained by considering horizontal gradients of T_b which could recognize mesoscale cloud structures and their relationship to precipitation.

The relative success obtained in transferring the algorithm is probably due to the similarity of climates in the developmental and test regions. Maritime soundings generally do not have the extreme variation found in continental climates (e.g., strong capping of low-level moisture by dry intrusions, dry line structures). One would, therefore, expect the precipitation efficiency to be more uniform in maritime environments. Second, surface boundary forcing is more uniform

than over land. Although sea-surface temperature patterns are probably important in modulating rainfall, complications arising from orography are absent. Application of the algorithm to a continental climate would almost certainly result in decreased performance. One might also expect a loss of skill in oceanic regions west of continents where semi-permanent anticyclones would maintain an environment with low precipitable water amounts. A more extensive test of these type problems is planned in future work.

The results presented in this paper have important bearing on future attempts at developing precipitation algorithms for oceanic climates. A large number of island stations in a variety of climates is available for use in constructing algorithms. Admittedly, possible problems of reporting accuracy and orographic influence cannot be discounted. Nevertheless, these data represent the most comprehensive measurement of precipitation available. Calibrated radar measurements, although preferable on the grounds of sampling capability, are much less readily available. Techniques which can take advantage of point measurements offer a means of extending indirect precipitation estimation schemes over middle-latitude oceans.

Acknowledgements

This study was supported by NASA contract NAS8-35187 and was begun when the author was supported under the Visiting Scientist Program by Universities Space Research Association. Precipitation data was supplied by Mr. Mike Changery at the National Climatic Center in Asheville, NC. GOES imagery was supplied by the Environmental Data Information Service at the University of Wisconsin, Madison, WI. The author also wishes to thank Dr. Dave Martin for providing additional SMS/GOES data from the GATE experiment. Ms. Fay Porter skillfully typed the manuscript.

REFERENCES

Arkin, P.A., 1979: The relationhip between fractional coverage of high cloud and rainfall accumulations during GATE over the B-Scale Array. Mon. Wea. Rev., 107, 1382-1387.

_____, 1983: A diagnostic precipitation index from infrared satellite imagery. Tropical Ocean Atmosphere Newsletter, 39, 5-7.

Emanuel, K., 1983: The Lagrangian parcel dynamics of moist symmetric instability. J. Atmos. Sci., 40, 2368-2376.

Griffith, C.G., W.L. Woodley, P.G. Grube, D.W. Martin, J. Stout and D.N. Sikdor, 1978: Rain estimations from geosynchronous satellite imagery - visible and infrared studies. Mon. Wea. Rev., 106, 1153-1171.

Hudlow, M.D. and V. Patterson, 1979: GATE Radar Rainfall Atlas. NOAA Special Report, Center for Environmental Assessment Services, NOAA, 155 pp.

Kilonsky, B.J. and C.S. Ramage, 1976: A technique for estimating tropical open-ocean rainfall from satellite observations. J. Appl. Meteor. 15, 972-975.

Lovejoy, S. and G.L. Austin, 1979a: The sources of error in rain amount estimating schemes from GOES visible and IR satellite data. Mon. Wea. Rev., 107, 1048-1054.

_____ and _____, 1979b: The delineation of rain areas from visible and IR satellite data for GATE and mid-latitudes. Atmosphere-Ocean, 17, 77-92.

Negri, A.J., R.F. Adler and P.J. Wetzel, 1984: Rain estimation from satellites: an examination of the Griffith-Woodley technique. J. Clim. Appl. Meteor., 23, 102-116.

Richards, F. and P. Arkin, 1981: On the relationship between satellite-observed cloud cover and precipitation. Mon. Wea. Rev., 109, 1081-1093.

Scofield, R.A. and V.J. Oliver, 1977: A scheme for estimating convective rainfall from satellite imagery. NOAA Tech. Memo. NESS 86, 47 pp. [NTIS PB270762/AS].

Spencer, R.W., 1984: "Satellite passive microwave rain measurement over croplands during spring, summer and fall. J. Clim. Appl. Meteor., 23, 1553-1562.

Stout, J.E., D.W. Martin and D.N. Sikdar, 1979: Estimating GATE rainfall with geosynchronous satellite images. Mon. Wea. Rev., 107, 585-598.

Vincent, D.G., 1985: Cyclone development in the South Pacicic Convergence Zone during FGGE, 10-17 January 1979. Quart. J R. Met. Soc., 111, 155-172.

Wilheit, T.T., A.T. Chang, M.S.V. Rao, E.B. Rogers and J.S. Theon, 1977: A satellite technique for quantitatively mapping rainfall rates over the ocean. J. Appl. Meteor., 16, 551-560.

Woodley, W.L., C.G. Griffith, J.S. Griffin and C.S. Stromatt, 1980: The inference of GATE convective rainfall from SMS-1 imagery. J. Appl. Meteor., 19, 388-408.

Wylie, D.P., 1979: An application of a geostationary satellite rain estimation technique to an extratropical area. J. Appl. Meteor., 18, 1640-1648.

Rain Rate Statistics		Pixel Indexing Method	Arkin (1979) Phase III Algorithm
n	sample size	11	11
R_o	mean observed rain rate mm/h	.57	.57
R_e	mean estimated rain rate mm/h	.55	.66
$\left\{\frac{\sum_1^n (R_o - R_e)}{n}\right\}^{1/2}$	root mean square error mm/h	.28	.22
$\frac{1}{n}\sum \frac{R_e}{R_o}$	bias	1.30	1.36
r	correlation coefficient	.85	.89

Table 1. Statistical summary of 12h-mean rainfall estimates produced over the GATE B-Scale Array during Phase III

Rain Rate Statistics		Pixel Indexing Method		Arkin (1979) Phase III Algorithm	
		12h Avg	24h Avg	12h Avg	24h Avg
n	sample size	8	16	8	16
R_o	mean observed rain rate mm/h	.80	.80	.80	.80
R_e	mean estimated rain rate mm/h	.92	.92	1.10	1.10
$\left\{\frac{\sum_1^n (R_o - R_e)}{n}\right\}^{1/2}$	root mean square error mm/h	.56	.36	.60	.46
$\frac{1}{n}\sum \frac{R_e}{R_o}$	bias	3.65	1.08	4.11	1.36
r	correlation coefficient	.71	.78	.73	.75

Table 2. Stastical summary of 12 and 24h-mean rainfall estimates produced over eastern North Carolina (see Fig. 4.)

Rain Rate Statistics		Pixel Indexing Method		Arkin (1979) Phase III Algorithm	
		Adjusted	Unadjusted	Adjusted	Unadjusted
n	sample size	16		16	
R_o	mean observed rain rate mm/h	.80		.80	
R_e	mean estimated rain rate mm/h	.99	.80	.72	.80
$\left\{\frac{\sum_{1}^{n}(R_o-R_e)}{n}\right\}^{1/2}$	root mean square error mm/h	.35	.30	.35	.34
$\frac{1}{n}\sum\frac{R_e}{R_o}$	bias	1.48	1.20	1.15	1.27
r	correlation coefficient	.74		.68	

Table 3. Statistical summary of 12h mean rainfall estimates produced at 43 island locations in the South Pacific Convergence Zone.

FIGURE CAPTIONS

Figure 1. Location of hourly-recording raingauges used in constructing algorithm.

Figure 2. Scatter diagram of hourly rain amount recorded at raingauge vs. equivalent black body temperature. Best fit 2nd-order polynomial is given by Eq. (1) in text. Also shown at top of diagram is percent of raingauge measurements reporting non-zero rain for 5^{o} K class intervals.

Figure 3. Rainfall rate over the GATE B-Scale array as estimated from EQ (1) and SMS-1/GOES IR data (shaded region) and determined from shipboard radar (Hudlow and Patterson, 1979) (dashed curve).

Figure 4. As in Fig. 3, except satellite estimate produced from GATE Phase III algorithm of Arkin (1979).

Figure 5. Hourly and daily reporting raingauge locations used to evaluate algorithms over North Carolina. Region enclosed by dashed line is area over which Eq. (1) was applied.

Figure 6. 12h rainfall rates over Coastal North Carolina for eight extratropical cyclone events. Shaded region is satellite estimate, solid line is raingauge measurement (see text for explanation). Left-hand panel: estimate from Eq. (1) right-hand panel: GATE Phase III algorithm (Arkin, 1979).

Figure 7. Forty-three Island raingauge locations used in evaluating algorithm performance over South Pacific.

Figure 8. 12h point rainfall rates averaged over the station location in Fig. 7. Actual raingauge measurement (solid line), satellite estimate using Eq. (1) (dashed line), satellite estimate using GATE Phase III algorithm (Arkin, 1979) (dotted line).

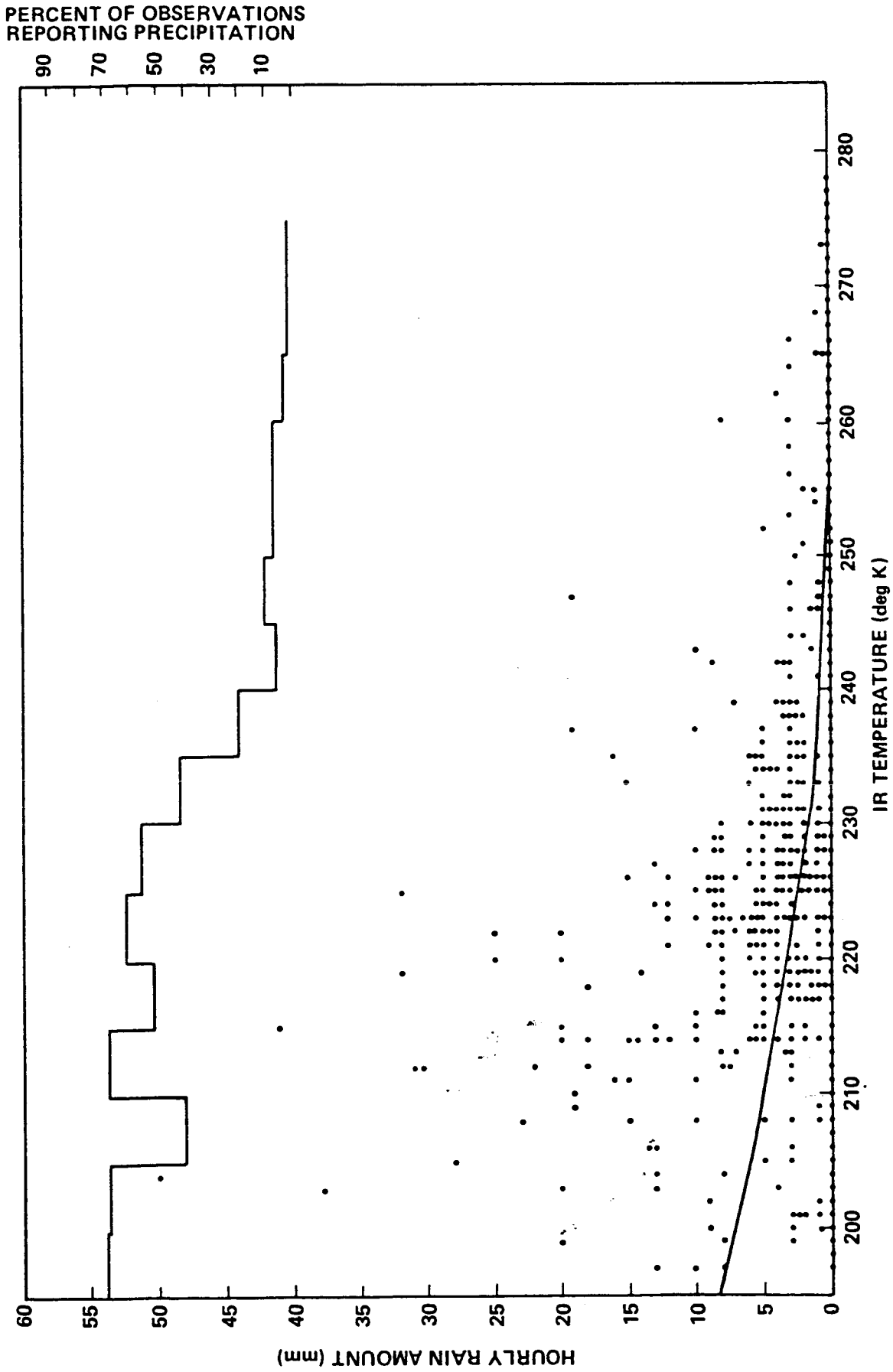
PERCENT OF OBSERVATIONS
REPORTING PRECIPITATION
90
70
50
30
10
HOURLY RAIN AMOUNT (mm)
60
55
50
45
40
35
30
25
20
15
10
5
0
IR TEMPERATURE (deg K)
200
210
220
230
240
250
260
270
280

Fig 1.

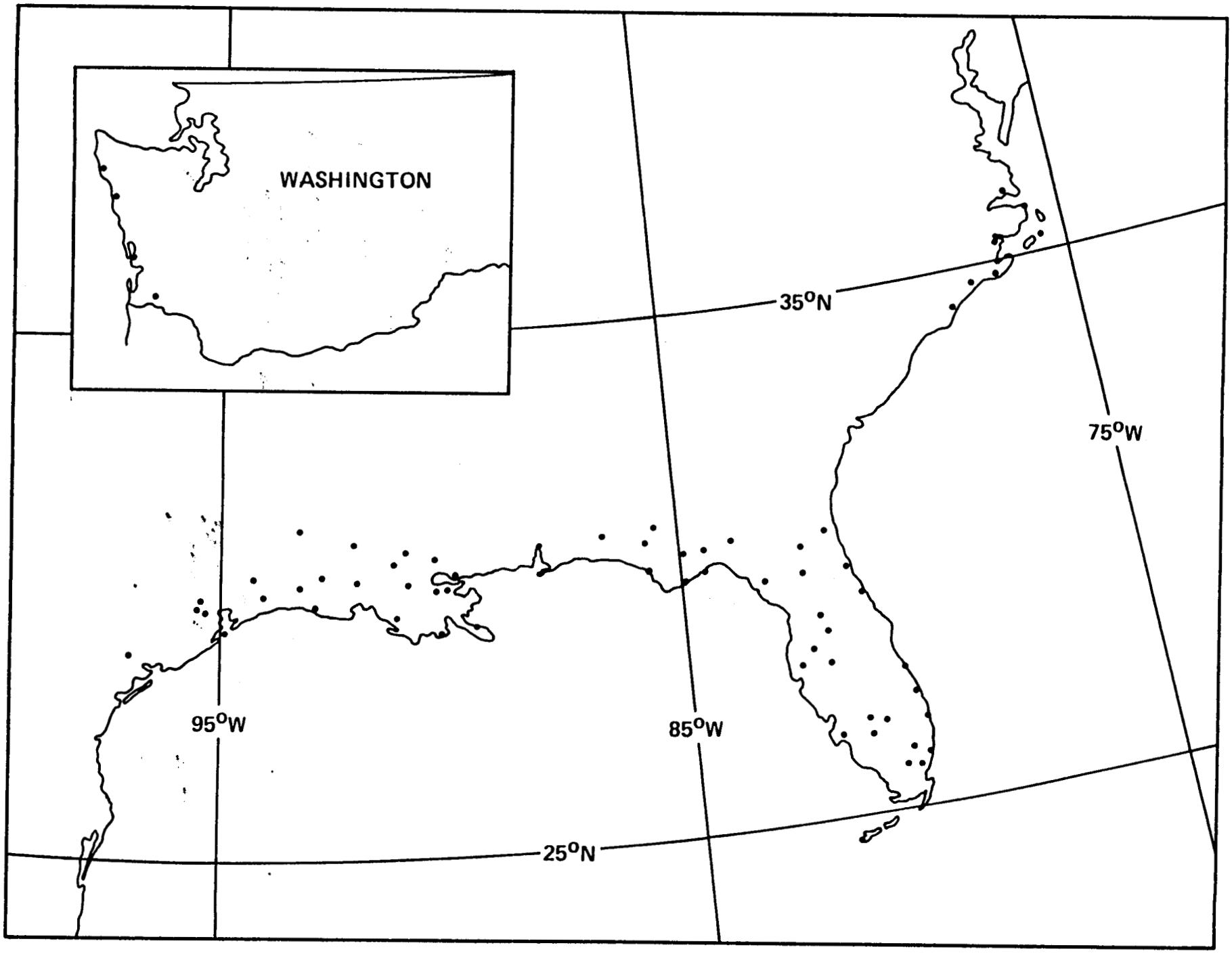

Fig 2.

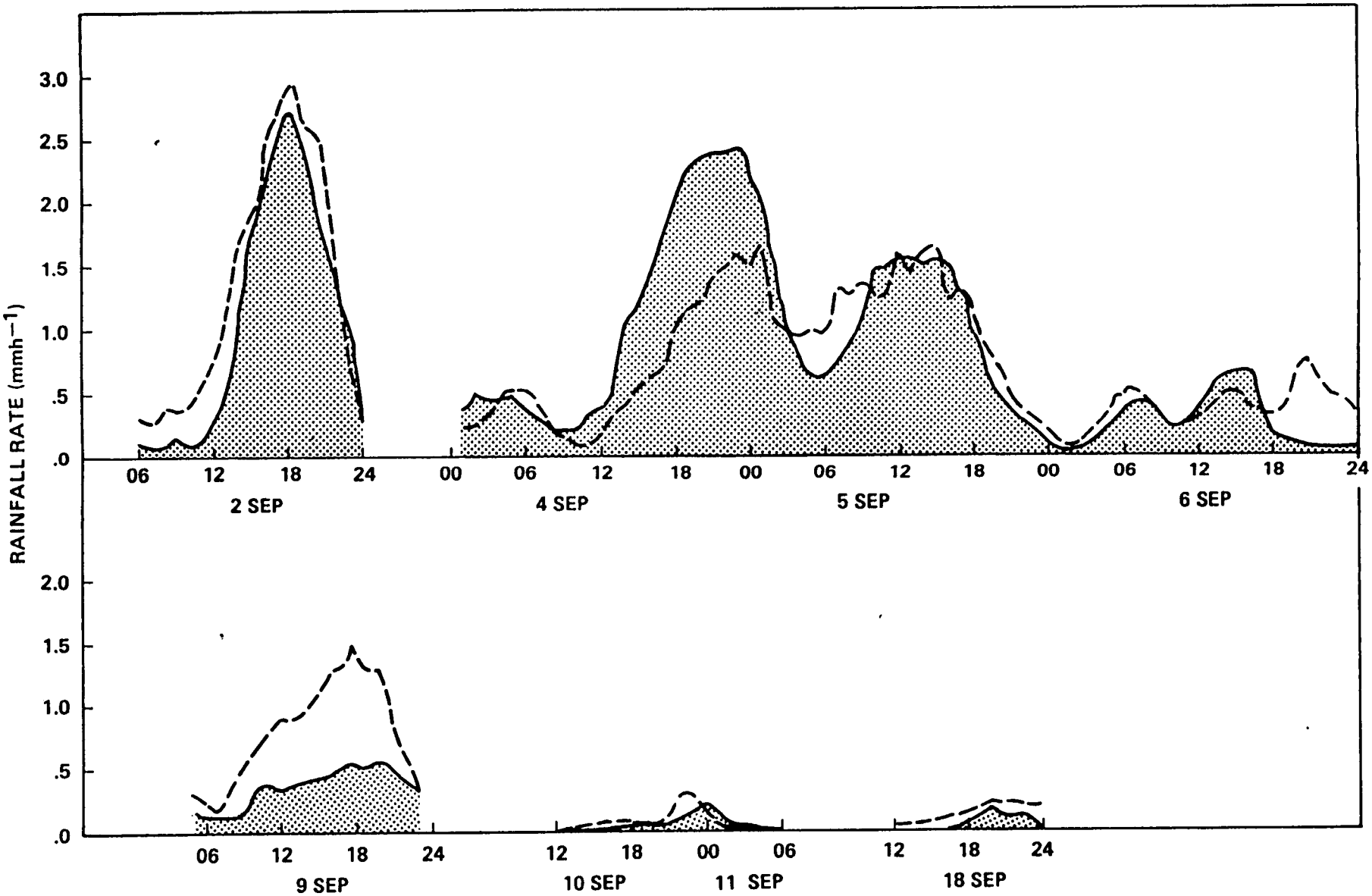
RAINFALL RATE (mmh⁻¹)
3.0
2.5
2.0
1.5
1.0
.5
.0
06
12
18
24
00
06
12
18
00
06
12
18
00
06
12
18
24
2 SEP
4 SEP
5 SEP
6 SEP
2.0
1.5
1.0
.5
.0
06
12
18
24
12
18
00
06
12
18
24
9 SEP
10 SEP
11 SEP
18 SEP

Fig. 3

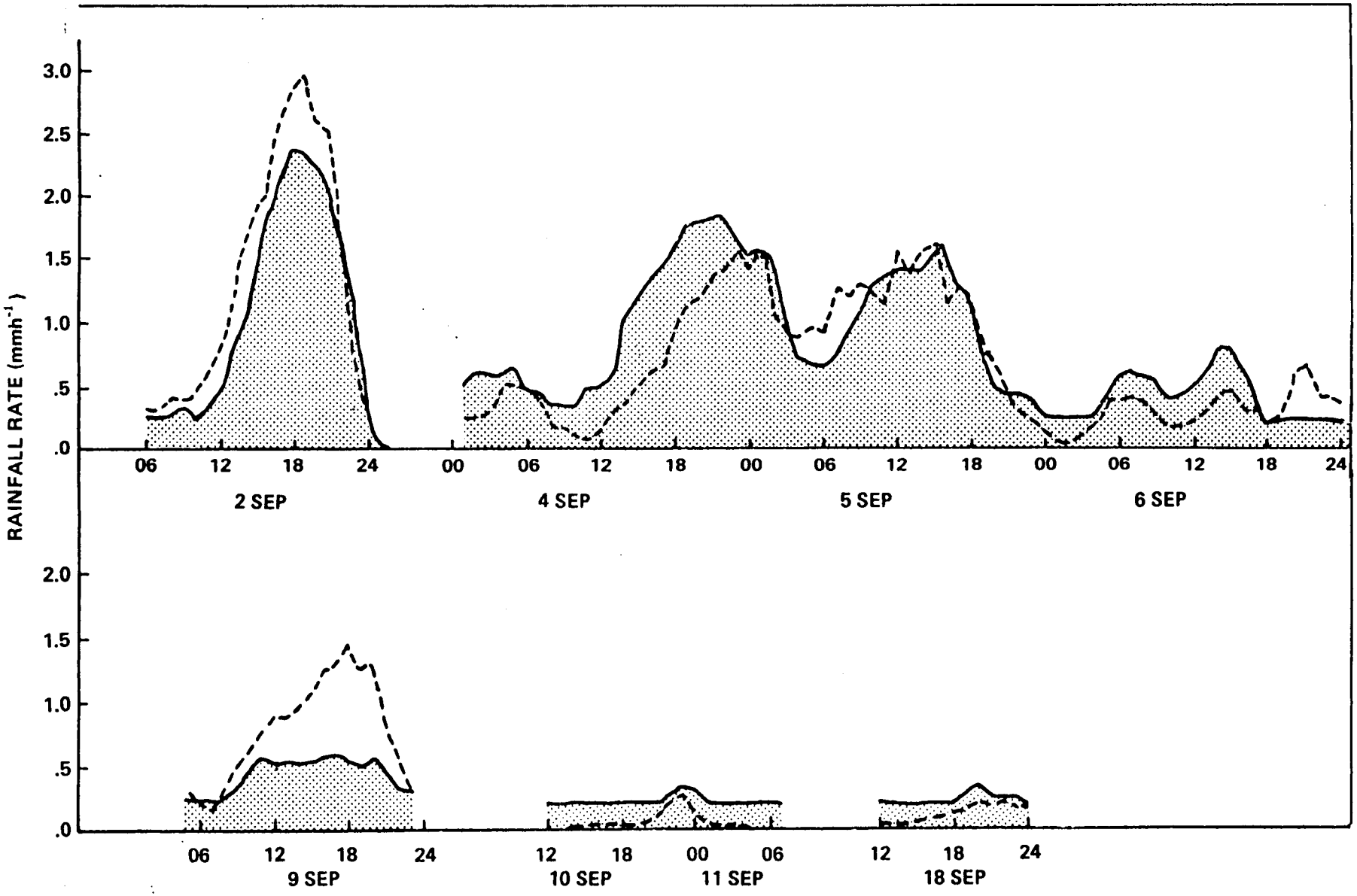
RAINFALL RATE (mmh^{-1})
3.0
2.5
2.0
1.5
1.0
.5
.0
06
12
18
24
00
2 SEP
4 SEP
5 SEP
6 SEP
9 SEP
10 SEP
11 SEP
18 SEP

Fig. 4.

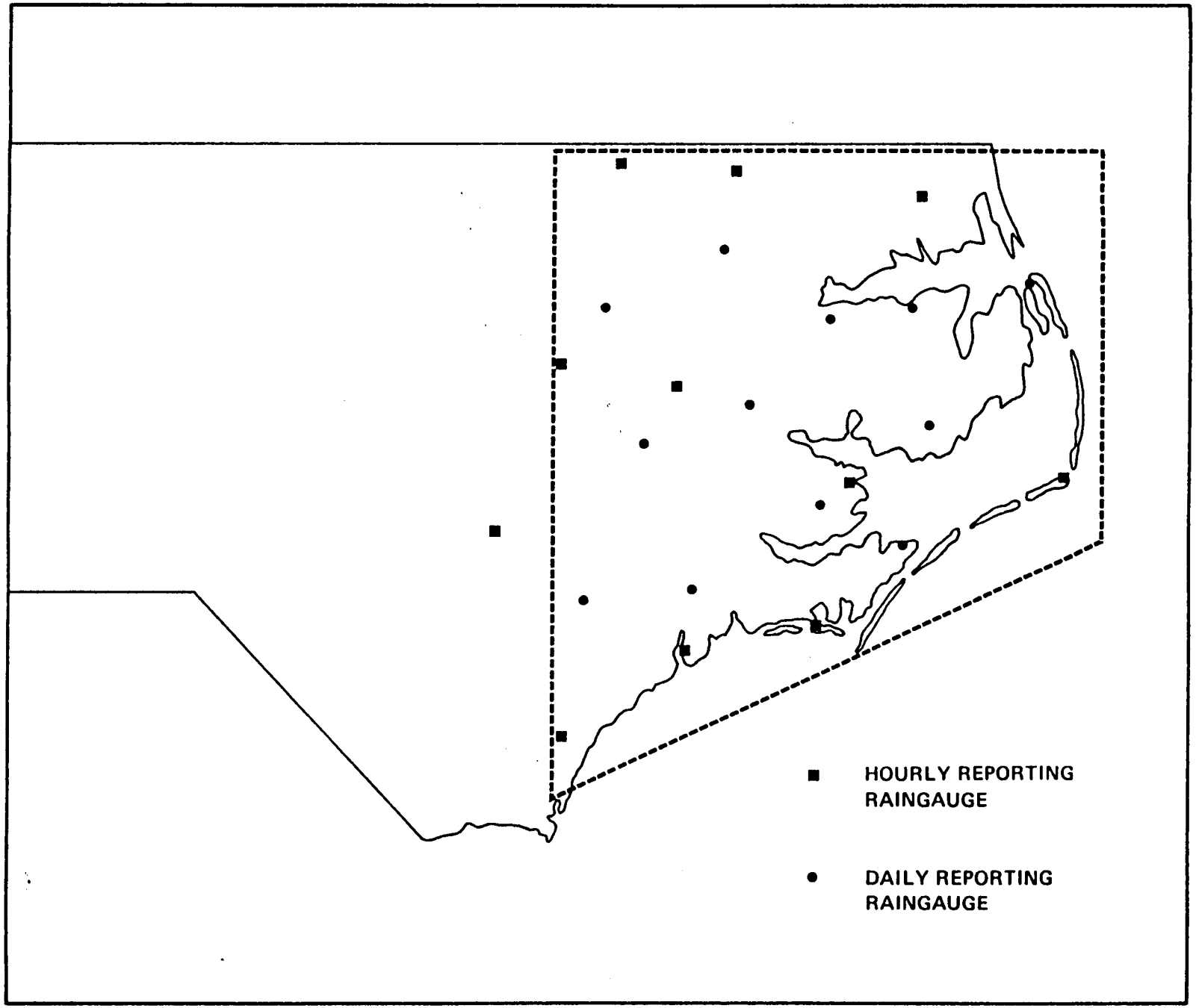

Fig. 5

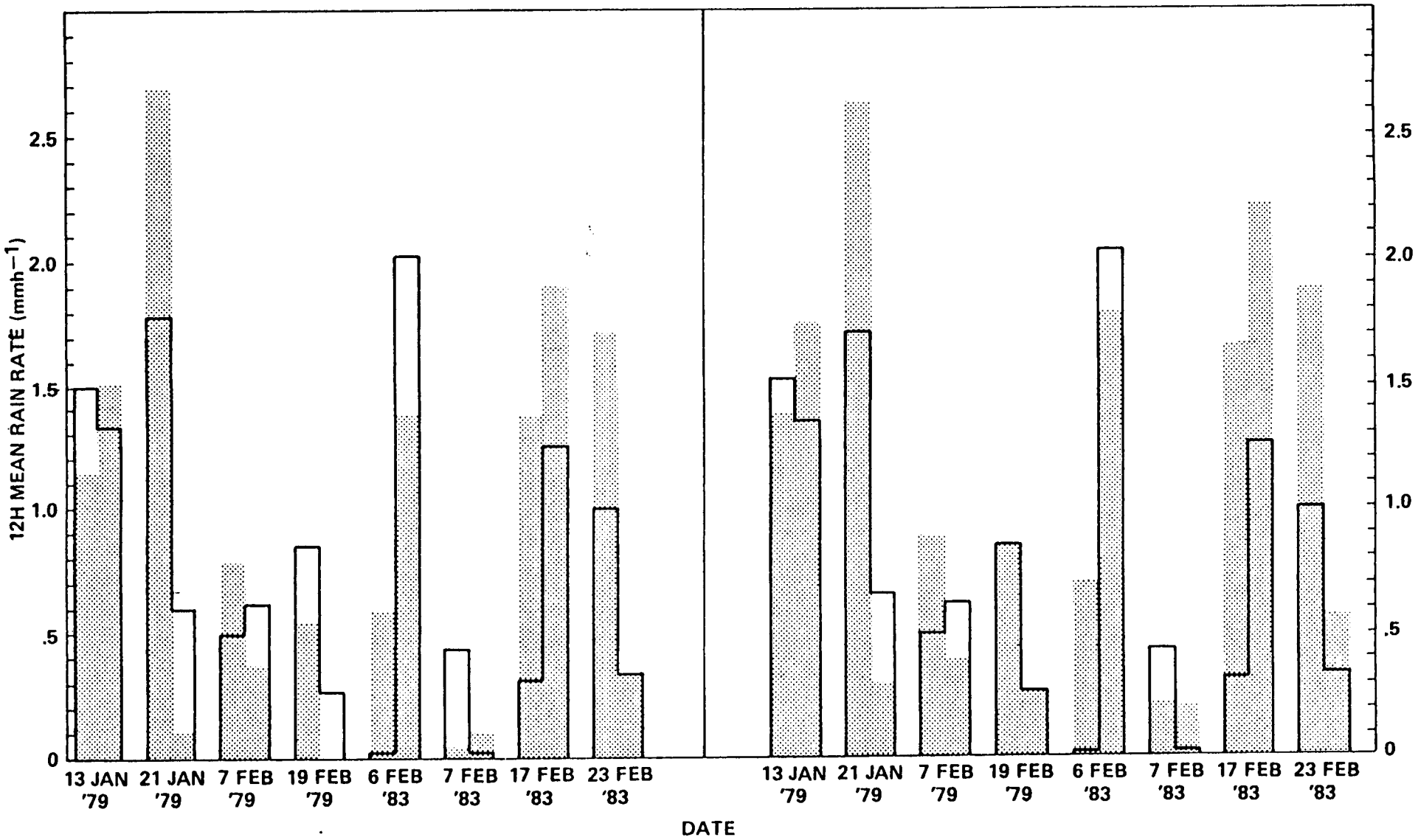
12H MEAN RAIN RATE (mmh^{-1})
2.5
2.0
1.5
1.0
.5
0
13 JAN '79
21 JAN '79
7 FEB '79
19 FEB '79
6 FEB '83
7 FEB '83
17 FEB '83
23 FEB '83
DATE

Fig. 6

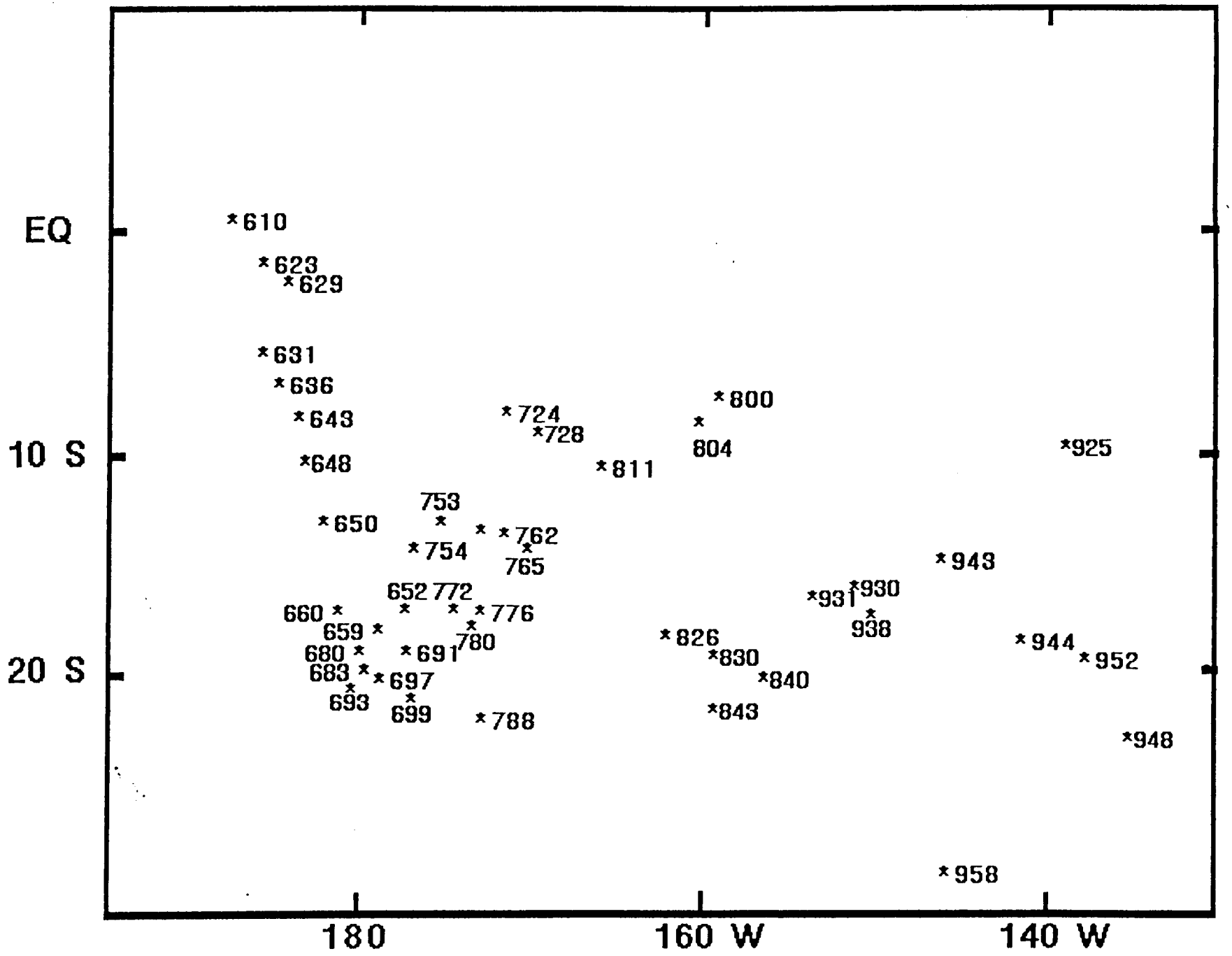
EQ
10 S
20 S
180
160 W
140 W
610
623
629
631
636
643
648
650
724
728
753
754
762
765
772
776
780
691
697
693
699
788
800
804
811
826
830
840
843
925
930
931
938
943
944
952
948
958
652
660
659
680
683

Fig. 7

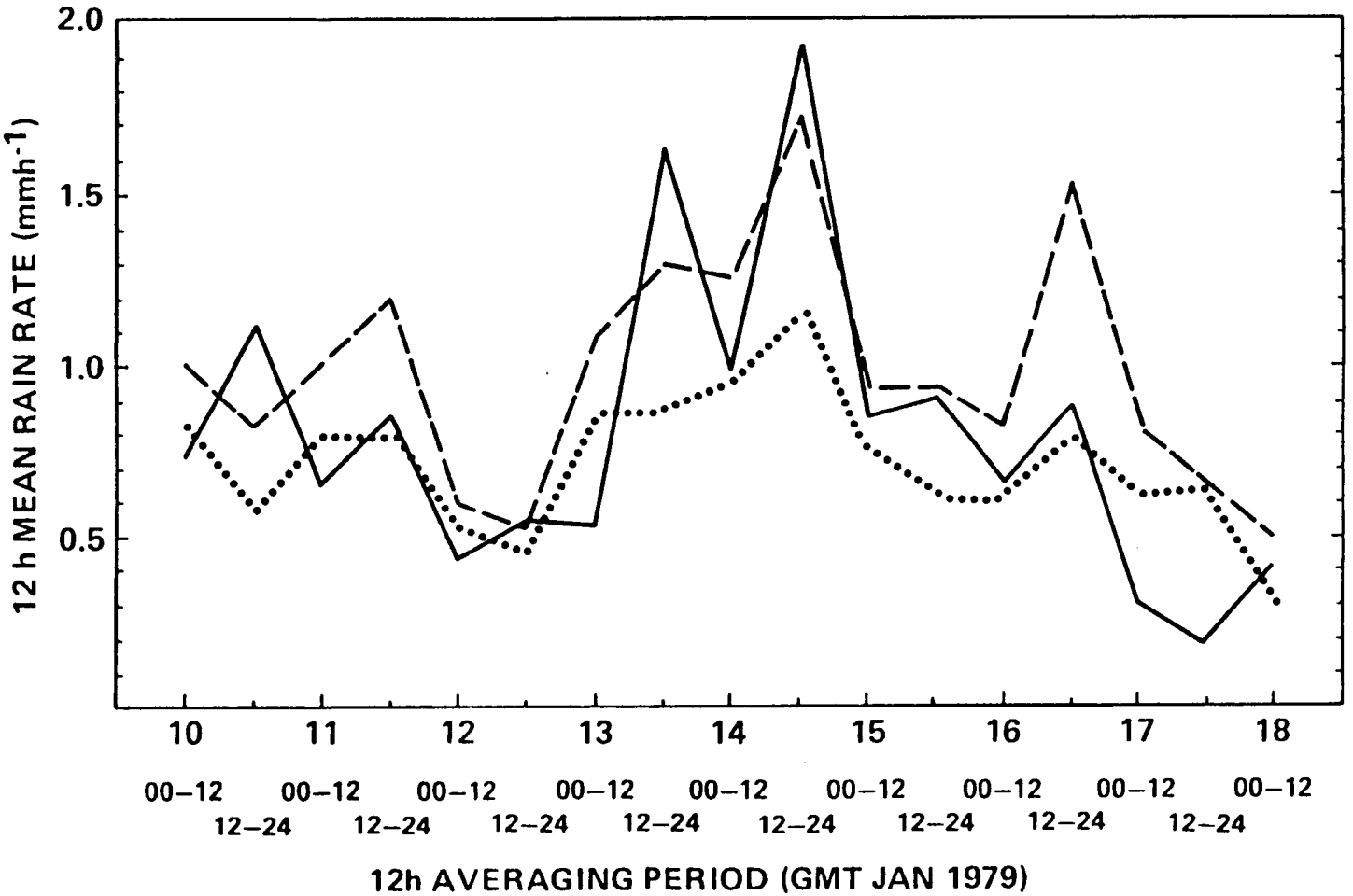
2.0
1.5
1.0
0.5
12 h MEAN RAIN RATE (mmh-1)
10
11
12
13
14
15
16
17
18
00–12
12–24
12h AVERAGING PERIOD (GMT JAN 1979)

Fig. 8